Lasers in Manufacturing Conference 2019

Dissimilar laser beam welding of press hardened stainless martensitic steels and a cold worked stainless TWIP steel

Martin Dahmen[a*], Berkan Deniz[a], Stefan Lindner[b], Dirk Petring[a]

[a]*Fraunhofer Institute for Laser Technology, Steinbachstraße 15, 52074 Aachen, Germany*
[b]*Outokumpu Nirosta GmbH, Oberschlesienstraße 16, 47807 Krefeld, Germany*

Abstract

Combinations of ultra-high strength and supra-ductile steels promise a multitude of benefits for steel construction in vehicle manufacturing. Laser beam welding is an appropriate tool for joining both materials due to its concentrated energy input. Results of research on laser beam welding of two press hardened steels, X46Cr13 (1.4034) and 37MnB5 (1.5538), and a dual phase steel DP980 (1.0944) to an X30MnCrN16-14 (1.4678), cold formed to 1000 MPa yield strength, will be reported. The resulting predominantly austenitic microstructure enables crack-free welding. Because of the cast structure in the weld material a loss of strength has to be considered. Hardness slopes in the heat affected zone of TWIP steel and significant softening in the press-hardened steel in conjunction with an inhomogeneous solidification structure in the fused zone leads to a complex strength profile in the weld zone. Insights will be given on microstructures, local chemical composition and hardness of the fused zone.

Keywords: Laser beam welding, TWIP steel, martensitic steel, microstructure, alloy composition, hardness

1. Introduction

High manganese TWIP steels offer great opportunities for vehicle construction. Excellent forming properties in conjunction with an increase in strength upon cold working enable efficient light-weight design components. In production energy can be saved by cold forming. Hence, an environmentally friendly product can be supplied. For assembly these steels have to be joined to other parts made from different grades. For joining the method of choice is laser beam welding in lap joint configuration. Intermixing of different

* Corresponding author. Tel.: +49-2418906307; fax: +492418906121.
E-mail address: martin.dahmen@ilt.fraunhofer.de.

materials will lead to local and varying changes in the alloy constitution and hence, may affect the mechanical properties of the joint.

Experiments have demonstrated (Behm et al. 2014, Behm et al. 2015) the formation of a martensitic phase in the dissimilar welds of TWIP HSD600 (with 0.7% C and 15.3% Mn, 1.7% Al, and 2.3% Si) to ferritic S420MC (1.0980) and dual phase steel DP 980 (1.0944). Depending on the mixing ratio of both materials, localised martensite was observed. As the austenite in the TWIP steel holds the carbon in solid solution in the ferritic steel large amounts of super-saturated austenite and martensite are formed. The most efficient microstructure to be obtained with overlap welds offering maximum shear forces, was that with the largest austenite fraction in the joining plane. It was emphasized that mechanical shear strength of the dissimilar welds was not better than that of the weakest alloy. Further studies on dissimilar butt joints of TWIP Fe-22Mn-0.6C to a TRIP800 (1.0943) (Mujica et al. 2010) reported segregation of manganese in the fused zone and subsequent martensite formation. Manganese segregations in the form of C-Mn precipitates have also been reported along the dendrite boundaries in a TWIP/TRIP butt joint close to the TWIP side (Rossini et al. 2015). Under tensile load, the latter butt joint fractured in the fusion zone. The resulting dissimilar joints exhibited poor mechanical strength. Tests on laser beam welding of a stainless TWIP steel (1.4678) to an austenitic-martensitic and a metastable austenitic stainless steel (1.4034 and 1.4301, respectively) have been reported by Dahmen et al. 2017. All fused zones solidify austenitic with martensitic streaks in regions with increased carbon content which fits well with the revised Schaeffler diagram suggested by Lee, Lee and Lee 2015. In the combination with the austenitic stainless steel the strength is determined by the weaker joining partner 1.4301. Fracture behavior of the combination with the press hardened martensitic stainless steel 1.4034 is more complicated. Failure is initiated at the fusion line but the crack propagates into the strong base material of 1.4034. The current state of the art indicates some demand of further research in order to understand the nature and effect of the metallurgy related to the intermixing in welds between high manganese TWIP steels and other grades.

Due to the random nature of melt flow during laser beam welding a strong variation of the local alloy constitution has to be expected. A variety of phases can be expected in the weld. During dedicated melting experiments Wittig et al., 2019 found austenite, ferrite, martensite α' and ε, and their mixtures depending on the actual alloy constitution. Martensite is controlled by the local manganese content and is expected at manganese contents above approximately 6 weight percent (Yang et al., 2015). The occurrence of these phases is also dependent on the strain state inside material (Scott, et al. 2005, Schumann, 1972)

For the phase assessment from the local alloy constitutions two approaches are available. The one of Lee, Lee, and Lee, 2015 comprises the results of Klueh, Masiasz and Lee, 1988, and is focused on the solid state transformations. The re-formulation of the equivalents for chromium and nickel, respectively, is restricted to the elements available in this work (equations 1 and 2):

$$Cr_{eq} = Cr + 2 \cdot Si \qquad (1)$$

$$Ni_{eq} = Ni + 0.5 \cdot Mn + 0.3 \cdot Cu + 25 \cdot N + 30 \cdot C \qquad (2)$$

A more recent approach by Wittig et al. 2017 has the advantage to map more exactly the welding situation, because the specimens were produced by direct quenching from the liquid phase. In an extension the approach also covers the conditions of rapid cooling supported by experiments on direct cooling from the melt phase (Wittig, Zinke and Jüttner 2019).

Welding in overlap configuration is the most frequently used design feature in car body and vehicle manufacturing. Given the requirements from application and regarding the state of the art an enhanced understanding of the microstructure and its constituents is essential in order to safeguard the quality as well as the mechanical stability of the weld. For this reason research has been undertaken to investigate the distribution and the properties of the fused zone in dissimilar lap welds with a cold formed TWIP steel as

base. The results will be used as a base for the assessment of the mechanical properties, but also constitute the fundamentals for the adjustment of, eventually required, thermal weld treatment.

2. Experimental

Steels under investigation are some structural steels used frequently in vehicle construction joined to stainless TWIP steel 1.4678, cold worked to a yield strength of 1 GPa. Low carbon steels are represented by a dual phase steel DP980. A press hardened manganese-boron steel with 0.37 weight percent carbon with an ultimate strength of 1900 MPa, was included in order to look at the effects of different carbon contents. By the application of an also press hardened stainless steel the effect of up to 0.46 wt.% carbon leaving the chromium content approximately constant at 14 weight percent. This steel was also press hardened to 2 GPa. All materials have been welded in uncoated state. Sheet thickness is 1.2 mm in the case of 1.4678 and 1.4036. The other materials had a thickness of 1.5 mm. Alloy compositions of the steels are given in table 1.

Table 1. Chemical analyses of the steels under investigation, contents given in weight percent

Material No.	Abbreviation	C	Si	Mn	Cr	Ni	Cu	V	N	others
1.4678	X30 MnCrN 16-14	0.3		16	14	0.2	0.5		0.3	
1.4034	X46 Cr 13	0.44	0.33	0.72	13.8	0.32	0.11	-	-	
1.5538	37MnB5	0.37	0.32	1.3	0.12	-	-	-		Ti, B
1.0944	DP 980	0.12	0.65	2.35	≤1	-	0.15	0.06	-	Mo, Ti

It is expected that the variation of the carbon content contributes to the formation of martensite, either as finely dispersed phase, which could increase the strength, or as coarse zones which can produce a notch effect and as such limit the strength of the weld.

Joining was carried out as autogenous laser beam welding at overlap joints. Welding was done in downhand (1G) position. The beam was generated by a disk laser and conducted by a fiber of 200 µm core diameter. It was focused by a lens optics with a focal length of 280 mm yielding a focal spot diameter of 286 µm. Beam power was set to 4 kW at a welding speed adjusted to the overall specimen thickness. Argon 4.6 was used as shielding and backing gas to prevent oxidation of the weld bead.

The welded specimens were at first investigated by metallographic inspection. Cross sections were taken by sectioning. The mounted specimens were sanded with up to P1200 (ISO 6344) before polishing them with diamond suspension. For contrasting different approaches had been applied. The stainless grades were etched by Kalling's reagent 2, whereas the welds to the unalloyed grades had been pre-etched by 3% Nital followed by electrolytic etching in diluted sodium hydroxide. Macrographs and detailed micrographs were taken by means of optical microscopy with up to 500-fold magnification.

Hardness measurement by low-load Vickers test applying a test load of 1.96 N (HV0.2), resulting in a maximum indentation width of 30 µm. A spacing of 100 µm was chosen. The measurements were taken across the seam at the center of the interface as well as in 0.2 mm distance above and below the interface in order to capture the hardness distribution of the weld, giving an indication about the strength of the weld.

In order to determine the chemical composition EDS measurements have been performed. As this method is sensitive to mass concentration greater than 0.3 weight percent for heavy elements (atomic number greater than 10) the contents of carbon and nitrogen have been calculated by linear interpolation taking the either values of the different parent materials as base. Obeying the chemical rules the relative content of nitrogen is calculated from the manganese content, that of carbon from the chromium content. The analysis was carried out at the same levels as the hardness measurement with a spacing of 29 µm.

For the assessment in the Schaeffler diagrams the approach suggested by Wittig et al., 2017 was applied. As chromium and nickel equivalents have to be applied:

$$Cr_{eq} = 1.2 \cdot Cr - 2.5 \cdot Si + 2.5 \quad (3)$$

$$Ni_{eq} = 1.3 \cdot Ni + 20 \cdot C + Mn \quad (4)$$

This revised version, called COHMS (**c**onstitution **o**f **h**igh **m**anganese **s**teel welds) fits well, as the approach considers the generation of the microstructure directly from the melt phase.

3. Results and discussion

3.1. Weld appearance, macro sections

All welds were crack-free and have shown little porosity. Their shape is slender with the typical Nail-shape. The average seam width ranges from 500 to 560 µm depending on the alloys and their thermophysical properties. At the joining interface a slight increase of width can be observed due to the thermal insulation and the flow of melt into the remaining gap.

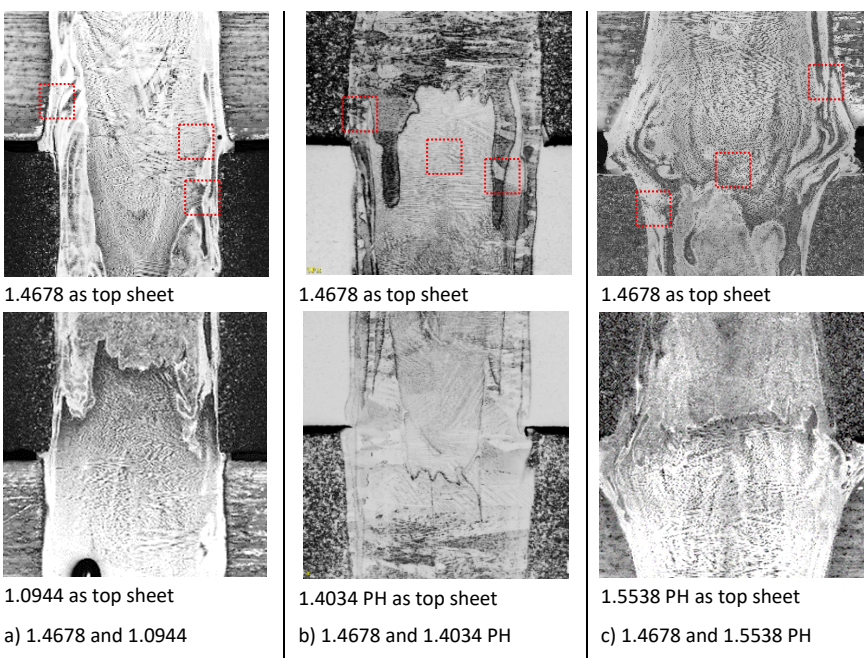

Fig. 1. Macrographs of the mid area of the weld showing different mixing patterns. Squares indicate the location of the micro-sections shown in figure 2.

Macro-sections were taken from the middle section from 0.4 mm below to 0.4 above the interface (figure 1). A complex flow pattern can be derived consisting of a mixture of boundary flow and free vortex mixing. From the intermixing of the material also areas with different micro-structures can be distinguished.

In the combination with the dual phase steel (fig. 1a) thin streaks of fresh martensite are visible in vicinity of the fusion lines. Fresh or tetragonal martensite is not etched by the reagents used. Hence, it appear as white in the microstructure. At the weld center line the austenitic structure indicates a strong flow of manganese-rich material, downwards when the TWIP steel is on top and upwards when it is at the bottom.

In the combination with the press hardened 1.4034 the structure of the fused zone consists predominantly of austentite with a little martensite at some of the fringes of the streaks (fig. 1b). In figure 1c a vortex-like structure is visible. A wide austenitic area at the weld center indicates a larger vertical vortex which decays in the region above the interface. There is also some transport from upside downwards. This can be seen at the narrow streaks of fresh martensite at the fusion lines in the TWIP steel.

3.2. Hardness

The full width hardness survey of the welds analyzed are shown in figure 2. In every weld a loss of strength of the 1.4678 can be observed as its hardness decreases from 500 HV0.2 to about 320 HV0.2 in the fused zone. The partner materials show a more or less pronounced tempering in the inter-critical zone of the HAZ and hardness peaks at the fusion line on the solid edge.

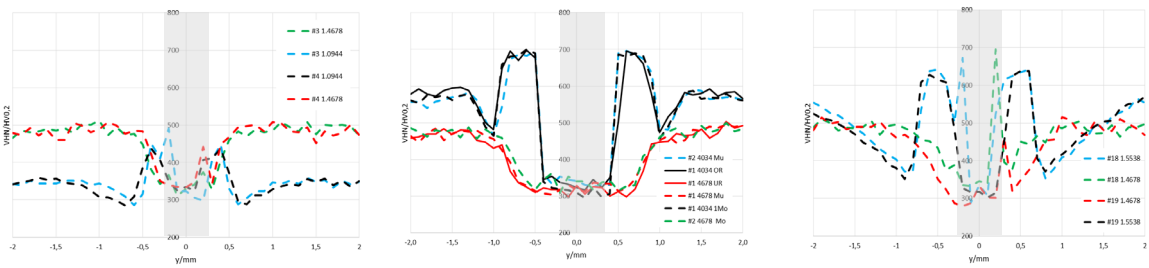

a) 1.4678 and 1.0944 b) 1.4678 and 1.4034 PH c) 1.4678 and 1.5538 PH

Fig. 2. Vickers hardness plots taken across the weld. Solid lines refer to the hardness at upper and lower surfaces. Dashed lines show the values at the levels 0.2 above and below the interface. Green and red lines refer to the track in 1.4678, blue and black lines refer the either joining partner. The space between the fusion lines is indicated as a grey shaded rectangle.

The hardness in the fused zone is determined by the contribution of manganese in the TWIP steel. Only in regions with low manganese content peaks in the hardness can be observed as in the combination with the dual phase steel (fig. 1a) and the manganese-boron steel (fig. 2c). As the streaks have a width of 40 to 60 µm they cannot all be covered by the hardness survey at a pitch of 100 µm. No peaks are visible in the combination with the 1.4034, although the average carbon content should be slightly increased. Its effect is neutralized by the austenite former manganese which holds the carbon in solid solution. The resulting hardness level is equal to that of the value of the recrystallized TWIP steel.

3.3. Microstructure

Enlarged micro sections have been taken from the configuration where the TWIP steel 1.4678 is on top of the joint. They are shown in figure 3 where the photographs from the top row are taken above the interface, those from the mid row directly on the interface, and the bottom row shows images from below the interface. The frame size is equal to 0.1 mm.

In the combination 1.4678/1.0944 the solidified structure is predominantly austenite. At the fusion line the white streaks of fresh martensite can be clearly seen (figure 3a). The reason for the comparably pronounced martensite formation is assumed in the mixing with the higher carbon containing TWIP steel in conjunction with dissolving carbon from the martensite islands in the dual phase steel. Due to its body-centered tetragonal structure this phase remains unetched as long as it is not tempered. Two of these streaks are separated by an austenitic region which seems to be solidified after the white areas are solidified.

At the right hand side of the photograph a bainitic region can be seen. At the weld center line (figure 3b) the microstructure is manly austenitic with two streaks of fresh martensite near the weld center line. In the region of the martensitic streaks the manganese content is less than 9 weight percent. Nitrogen was calculated to be maximum 0.15 weight percent. The presence of martensite can be also confirmed by hardness measurement, as shown by the dashed blue and red curves in figure 2a. The other streaks could not have been detected due to the relatively coarse resolution of the hardness track. At the fusion line to the dual phase steel a layered structure of martensite, austenite, and again martensite occurs as visible from figure 3c.

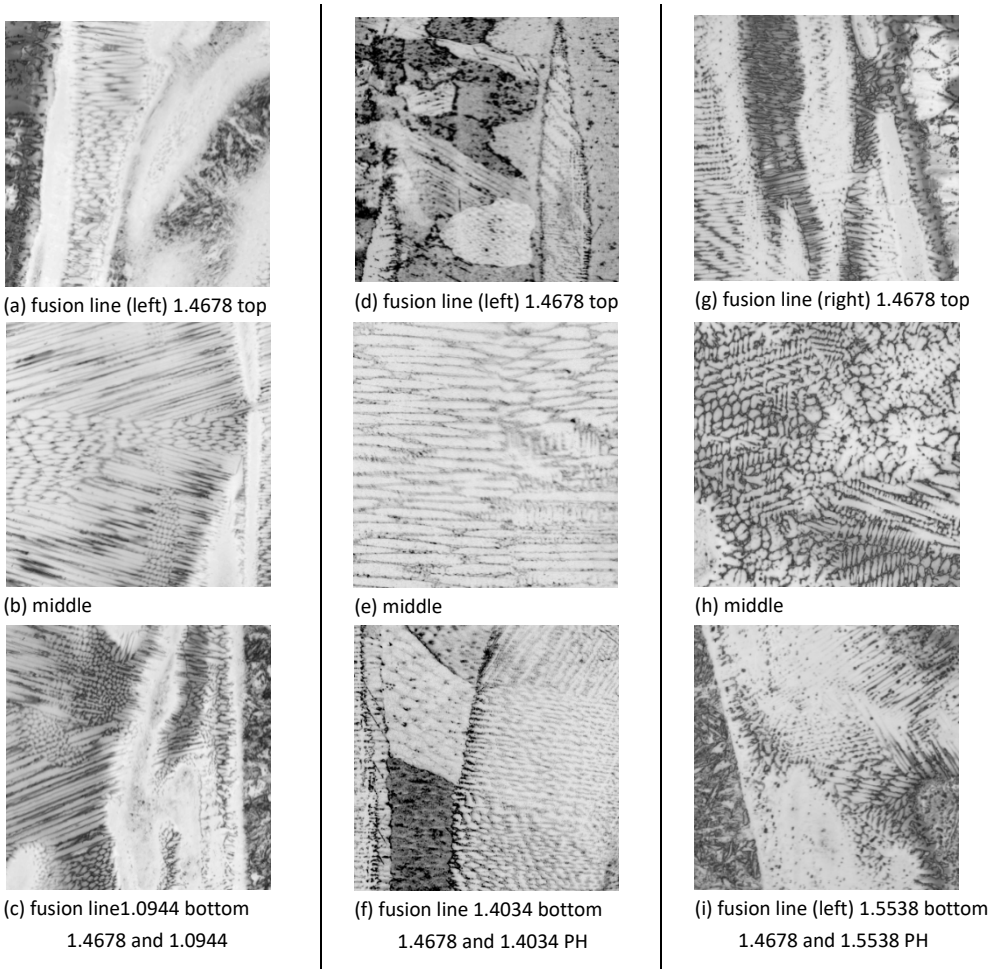

(a) fusion line (left) 1.4678 top
(d) fusion line (left) 1.4678 top
(g) fusion line (right) 1.4678 top
(b) middle
(e) middle
(h) middle
(c) fusion line1.0944 bottom
1.4678 and 1.0944
(f) fusion line 1.4034 bottom
1.4678 and 1.4034 PH
(i) fusion line (left) 1.5538 bottom
1.4678 and 1.5538 PH

Fig. 3. Micro-sections of different zones of the fused zone. The frame width is equal to 100 µm.

The combination with 1.4034 (figure 3 d, e, f) shows a mainly austenitic microstructure. Some martensite can be found at the grain boundaries in the fused zone near the fusion line in the TWIP steel (top). At the section between interface and weld center line four austenitic columnar grains meet without separating phases between them (figure 3e). The pattern at the fusion line in 1.4034 is characterized by curved flow patterns and austenitic solidification (figure 3f). The fully austenitic microstructure is confirmed by the hardness plot shown in figure 2b. In the area of the streaks manganese rich material is pushed downwards.

As a consequence the solidified structure maps the local alloy constitution. Smaller columnar grains indicate more manganese in contrast to chromium and carbon dominant larger dendritic grains.

Fig. 4. Results of the local chemical analysis of the composition of the fused material 0.2 mm above the interface (top), at the interface (middle), and 0.2 mm below the interface (bottom).

Martensite formation concentrates on the level of the manganese boron steel (1.5538), mainly in the vicinity of the fusion lines (figure 3g). Single streaks of fresh martensite visible at some boundaries between austenitic and martensitic material. They correspond with a composition of 7% Mn, 6.5% Cr, and 0.15% N and are also visible as the hardness peaks, seen in figure 2c. The austenitic regions in the center correspond with a composition of 12% Mn and 0.25% N minimum. Streaks of austenite in the 1.5538 indicate the presence of manganese at a content of above 10 weight percent. Indications of cracks were found at some boundaries between fresh martensite and austenite, but also within some austenite dendrites (figures 3 h, i). A possible explanation for their occurrence might be the difference of the thermal expansion coefficients, which amount in manganese rich steel to up to $22 \cdot 10^{-6} K^{-1}$ compared to that of unalloyed steel of $13 \cdot 10^{-6} K^{-1}$ (Bhattacharya, 2018). For steel with a manganese content of up to 6 weight percent Yang et al., 2015 determined a linear thermal expansion coefficient of $10 \cdot 10^{-6}$ to $15 \cdot 10^{-6} K^{-1}$. Different thermal expansion of adjacent cells may lead to separation of their boundaries during solidification. Also a difference in solidification temperature and interval from 1520°C for Fe-C to 1380°C for the alloy 1.4678 and a slight increase of the solidification interval for the high manganese steel may contribute to this effect at the high cooling rates in laser beam welding.

3.4. Element distribution

The results of EDS analyses across the fused zone are depicted in figure 4. The diagrams show the concentrations of manganese and chromium on the primary, those of carbon, nitrogen, and silicon on the secondary vertical axes across the weld. In this analysis a configuration with the 1.4678 in bottom position was taken. For the top and bottom lines the measurement track starts and ends in the either base material whereas in the middle level only the fused material was analyzed. A shaded area indicates the interval between 6 and 10 weight percent manganese, where the onset of martensite is assumed. Comparing the graphs to the macro-sections the different zones revealed by metallography are well congruent with the element distribution.

Figure 4 a to c show the distribution of elements in the combination 1.0944/1.4678 (dual phase steel in top position). In the top sheet a local increase of manganese and chromium to 14 and 12 weight percent, respectively, is visible in the central section of the weld. By metallographic inspection this area was determined to be austenitic. In the vicinity of the fusion line a dip in the manganese content can be seen. These areas correspond to the martensitic streaks visible in the macro-section in the lower row of figure 1a. The outer edges towards the fusion line are dominated by the original composition. This holds also true for the middle and bottom level, where the fusion line is covered by an epitaxial layer of solidified unalloyed steel. These bainitic or martensitic areas are found if the concentration of manganese is below 10 weight percent.

In the combination with 1.4034 the chromium content is constant due to the actual alloy compositions of both materials. Carbon varies slightly around the average mixing ratio of 0.38 weight percent. The manganese rich streaks visible in the macro section in figure 1b can be tracked by the peaks in the contents of manganese and nitrogen. The overall microstructure is austenitic (fig. 3 d to f). Obviously the condition of a manganese content greater than 10 weight percent is not valid in this alloy system. Some carbides are found on the grain boundaries, mainly along the streaks near the fusion lines in the 1.4678 (fig 3d).

Analysis of the actual cross section of 1.5538/1.4678 (fig. 4g to h) shows a similar distribution of elements as the combination with 1.0944 but a limited intermixing. The take-up of chromium and manganese in the part of the manganese-boron steel is limited to maximum 4 weight-percent. The carbon content remains constant whereas the nitrogen is slightly increased. At the middle level both major elements show a nearly constant distribution except in a region of the streak at y = 0.35 mm. The same holds for the lower level at increase values for manganese and chromium which are found, at concentrations of 14 and 12 weight percent, respectively (figure 4f).

3.5. Comparison with COHMS diagram

In Figure 5 the equivalents for chromium and nickel calculated from the local EDS analysis using formulas (3) and (4) are inserted into the COHMS diagrams. Here the joints where the TWIP steel is the top sheet are considered. The base materials are indicated by shaded ellipses, red for the TWIP steel 1.4678 and green for the either partner materials. Except for the dual phase steel the local values measured in the fused zone are found along a straight line connecting the base metal values.

Figure 5a shows the COHMS diagram for the combination of TWIP and dual phase steel. A homogenous mixing is indicated for the upper and middle part of the weld. In the lower part of the weld of the TWIP and the dual phase steel kind of a bifurcation is seen. The points around the nickel equivalent of about 17% belong to the central part of the fused zone whereas those at lower values correspond with the martensitic streaks. The prediction of the microstructures is in good agreement with the metallographic findings as well as the hardness is.

The 1.4034 is found in the undefined region of the COHMS diagram given in figure 5b. In the diagram by Lee, Lee and Lee, 2015, the alloy is supposed to be in a region where γ, α', and α or δ are predicted. It is assumed that the latter are suppressed by the action of the high carbon content. The ε carbides, as predicted in the diagram (fig 5b) could not be detected. As the metallographic inspection shows a fair intermixing there is a gradual transition towards the pure austenitic 1.4678. Regarding the values in the fused zone the hardness values fit with those given in the diagram.

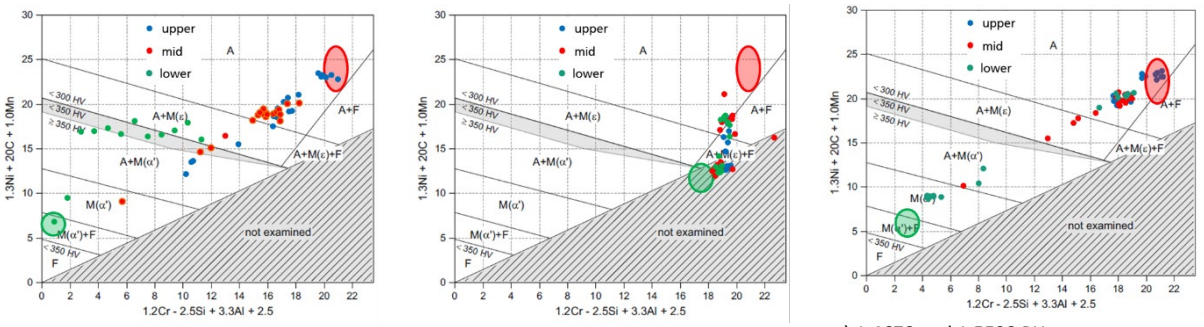

a) 1.4678 and 1.0944 b) 1.4678 and 1.4034 PH c) 1.4678 and 1.5538 PH

Fig. 5. Rating of the three materials and the fused zone mixtures in the COHMS diagram

From the macro-sections of the weld between 1.4678 and 1.5538 (figure 1c) a clearer separation was seen than for the other combinations. In figure 5c this seems only to be true for the upper part of the weld. For the other areas the values for chromium and nickel equivalents spread over the whole range between the either base materials indicating mixing in the middle level and the austenitic streaks near the fusion lines of the manganese boron steel as revealed from the micro-sections in figure 3c. These streaks are also visible in the element distribution and as peaks in the hardness curve. In the COHMS diagram these three points are located in the band of maximum hardness.

4. Conclusions and outcast

A study was undertaken in order to research the details of metallurgy in dissimilar welds of a stainless TWIP steel to other ultra-high strength steels. The element distribution and the resulting microstructures are determined by a complex flow pattern most probably consisting of an alternating flow around the keyhole, downward transport of melt along the keyhole front, and vortex flow and shedding in the wake driven by vapor pressure gradients as well as Marangoni and buoyant flow.

In combinations with the dual phase and the manganese boron steels the bond area of 0.2 mm above and below the interface is characterized by an austenitic microstructure as the manganese content supersedes 10 weight percent. Between 6 and 10 weight percent martensite is formed found in streaks of 40 to 60 µm width. Another source of untempered martensite is an epitaxial layer at the fusion lines in the unalloyed materials. This leads to an inhomogeneous distribution which can be considered as a measure for the tensile strength. It ranges between 320 and 650 HV0.2, where the maximum hardness peaks are measured in the combination with the press hardened manganese boron steel. The weld in the combination to the press hardened stainless martensitic steel is austenitic. Its hardness ranges around 330 HV0.2. Micro-sections of selected zones in the weld confirm these findings.

The COHMS diagram was proven to be an appropriate tool for microstructure prediction in the case of combinations with the unalloyed grades. In case of an increased carbon content some re-fit was determined. Hardness values do not correlate neither with chromium nor with the nickel equivalent alone. A projection

onto a transformed x-axis using $\sqrt{Ni_{eq}^2 + Cr_{eq}^2}$ corresponds qualitatively better and gives reasonable results in the case of the combination with 1.0944.

As the methods applied have a limited resolution further investigations are planned considering local measurements of the chemical composition and hardness assessment by nanoindentation based on the actual microstructures. From this approach a detailed understanding of the metallurgy and its effect on the mechanical properties is expected. Within the frame of mechanical testing and fractographic analysis the contribution of different microstructural constituents and their distribution to the weld strength will be determined.

Acknowledgements

The authors would like to thank the research partners and research association for their contribution to the presented results. This work is part of the research project „Weiterentwicklung, fügetechnische Absicherung und technische Auslegung von Schweißverbindungen mit martensitischen Chromstählen", IGF-project No. 19556 N, of the Research Association for Steel Application (FOSTA), which is funded by the AiF as part of the program for "Joint Industrial Research (IGF)" by the German Federal Ministry of Economics and Technology (BMWi) by decision of the German Federal Government.

References

Bhattacharya, D.,2018: Liquid metal embrittlement during resistance spot welding of Zn-coated high-strength steels, *Materials Science and Technology*, 34:15, p. 1809

Behm, V., Höfemann, M., Hatscher, A., Springer, A., 2014: Investigations on laser beam welding dissimilar material combinations of austenitic high manganese (FeMn) and ferrite steels, *Physics Procedia* 56, p 610

Behm. V.,Hoffman, G., von Trzebiatkowski, J., Springer, A., Kaierle, S., Overmeyer, L., 2015: Method for evaluating the behavior of laser welded dissimilar material seams in single overlap configuration under impact loads by the example of twinning induced plasticity steels, *Journal of Laser Applications* 27, S29006, doi: 10.2351/1.4906384

Campangoli, E.; Matteis, E.; Mortarino, G., Scavino, G., 2010: Thermal diffusivity of traditional and innovative sheet steels. Defect and Diffusion Forum, Vol. 297-301, p. 893

Dahmen, M., Lindner, S., Petring. D., 2017: Perspectives of laser-beam welding of ultra-high strength steels, *Proceedings of the Conference on Lasers in Manufacturing*, June 26-29, Munich, contribution #251

Klueh, R., Masiasz, P., Lee, E., 1988: Manganese as an austenite stabilizer in Fe-Cr-Mn-C steels. *Materials Science and Engineering* A 102, p. 115

Lee, S., Lee, C., Lee, Y., 2015: Schaeffler diagram for high Mn steels. *Journal of Alloys and Compounds* 628, p. 46 – 49

Mújica, L. Weber, S., Pinto, H., Thomy, C., Vollertsen, F., 2010: Microstructure and mechanical properties of laser-welded joints of TWIP and TRIP steels, *Materials Science and Engineering* A527, p. 2071

Rossini, M., Russo Spena, P. Cortese, L., Matteis, P., Firrao, D., 2015: Investigation on dissimilar laser welding of advanced high strength steel sheets for the automotive industry, *Materials Science & Engineering* A628, p. 288

Schumann, H., 1972: Distribution of phases in Fe-Mn-C system after deformation, Neue Hütte 17, p. 605.

Scott, C., Guelton, N., Allain, S., Faral, M., 2006: The development of a new Fe-Mn-C austenitic steel for automotive applications, *Revue de Métallurgie*, June, p. 293, doi: 10.1051/metal:200614

Wittig, B., Zinke, M., Jüttner, S., Keil, D., 2017: Experimental simulation of dissimilar weld metal of high manganese steels by arc melting technique, *Welding in the World* 61, p.249

Wittig, B., Zinke, M., Jüttner, S., Keil, D., 2018: A new constitution diagram for dissimila metal welds of high manganese steel, *Welding in the World* 63, p. 491

Wittig, B., Zinke, M., Jüttner, S.: Martensite formation in dissimilar weld metals of high-Mn steels, *Proceedings of The 4th International Conference on Medium and High Manganese Steels*, April 1-2, 2019, Aachen, p. 271

Yang, J., Wang, Y., Ruan, X., Wang, R., Zhu, K., Fan, Z., Wan, Y., Li, C., Jiang, X., 2015: Effects of manganese content on solidification structures, thermal properties, and phase transformation characteristics in Fe-Mn-C Steels, *Metallurgical and Materials Transactions*, 46 B, DOI: 10.1007/s11663-015-0297-y